Physics Letters B 745 (2015) 79–89

Contents lists available at ScienceDirect

Physics Letters B

www.elsevier.com/locate/physletb

A measurement of the neutron lifetime using the method of storage of ultracold neutrons and detection of inelastically up-scattered neutrons

S. Arzumanov [a], L. Bondarenko [a], S. Chernyavsky [a], P. Geltenbort [c], V. Morozov [a,b], V.V. Nesvizhevsky [c,*], Yu. Panin [a], A. Strepetov [a]

[a] NRC "Kurchatov Institute", 1 Akademika Kurchatova sqr., Moscow, R-123182, Russia
[b] NRNU MEPHI, 31 Kashirskoe sh., Moscow, R-115409, Russia
[c] Institut Max von Laue–Paul Langevin, 71 av. Martyrs, Grenoble, F-38042, France

ARTICLE INFO

Article history:
Received 29 July 2014
Received in revised form 24 March 2015
Accepted 11 April 2015
Available online 21 April 2015
Editor: M. Doser

ABSTRACT

We present estimations of systematic corrections and results of their experimental studies for our neutron lifetime experiment carried out in 2008–2010 at ILL. Taking into account these systematic corrections, we reduce the data of three independent sets of measurements (obtained during period 2008–2010) performed with different energy spectra of ultracold neutrons (UCNs) at different trap temperatures to the mean neutron lifetime value equal to 880.2(1.2) s.

1. The experimental installation and the method

Precise measurements of the neutron lifetime are important for elementary particle physics, astrophysics and cosmology [1,2]. In accordance to Particle Data Group (PDG) [3], the neutron mean lifetime world value is estimated using works [4–11]; it is equal to 880.3 ± 1.1 s.

The main contribution to the mean world value comes from work [6], which uses the method of storage of ultracold neutrons (UCNs); its result is $\tau_\beta = 878.5 \pm 0.7_{\rm st} \pm 0.3_{\rm meth}$ s. Other results using this method [4,5,7,8] are significantly less precise; uncertainties in these experiments are 2–3 s. Main limitations of the UCN storage method are related to systematic corrections.

The probability of UCN loss from a trap $\lambda = \lambda_l + \lambda_\beta$, where $\lambda_l = p\mu$ is the probability of UCN loss in the trap walls, $\lambda_\beta = 1/\tau_\beta$ is the probability of neutron decay, p is the frequency of UCN collisions with the trap walls, and μ is the probability of UCN absorption and inelastic scattering per bounce.

UCN storage experiments were often based on measuring the probability λ in two or several traps with equal values of μ and different frequencies p, which were calculated in accordance with certain assumptions about the behavior of UCNs in traps [6–8]. Then, λ_β was evaluated by linearly extrapolating the experimental data $\lambda(p)$ to the zero frequency $p = 0$. Within this approach, systematic corrections are related to the validity of the condition of equality of μ in the traps as well as to the accuracy of calculations of the frequency p.

Within an alternative approach [4], not only the probability λ, but also the probability λ_l were measured experimentally; the probability λ_l was measured in relative units using the flux of thermal neutrons originating from UCNs up-scattered on trap walls. Then, λ_β was evaluated by linearly extrapolating the experimental data $\lambda(\lambda_l)$ to the zero probability $\lambda_l = 0$. Systematic corrections inherent for this approach are related to the differences in the efficiency of detection of UCNs and thermal neutrons originating from UCNs up-scattered on trap walls.

Recently, results of many UCN storage experiments were largely shifted or selected a posteriori due to additional analysis or new data. Moreover, results of measurements using the method of UCN storage [4–8] and those using the method of in-flight decay of cold neutrons [9–11] differ by many seconds. Thus, the most precise in-flight experiment [11] provides the value of neutron lifetime $\tau_\beta = 887.7 \pm 1.2_{\rm st} \pm 1.9_{\rm meth}$ s that differs from the result [6] by 9.2 s, by far larger then the estimated uncertainties of these experiments. Apparently this difference is caused by systematic effects, which have not been properly identified. Therefore new neutron lifetime experiments with the accuracy of at least ~1 s (equal to the world average), and also with a reliable accounting for systematic effects is highly desirable.

The neutron lifetime experiment using storage of UCNs in traps and detection of neutrons, escaping from the storage trap via their

* Corresponding author.
E-mail address: nesvizhevsky@ill.eu (V.V. Nesvizhevsky).

http://dx.doi.org/10.1016/j.physletb.2015.04.021

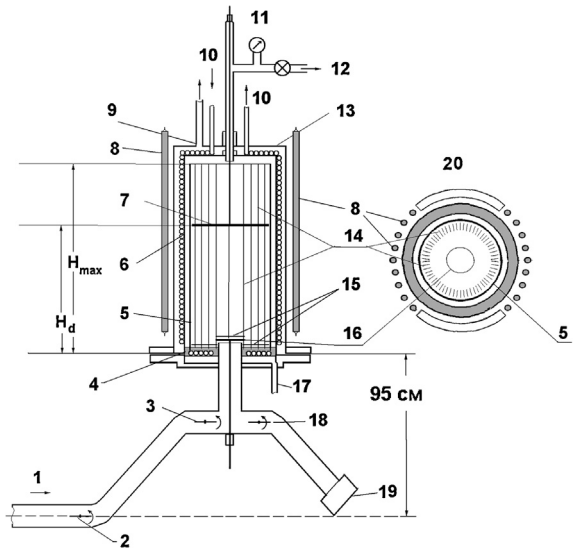

Fig. 1. A scheme of the experimental set-up for the neutron lifetime measurement. 1 – the entrance neutron guide, 2 – the UCN source shutter, 3 – the input shutter, 4 – fluid fluorine polymer, 5 – the copper cylinder, 6 – the cooling coil, 7 – the polyethylene disk, 8 – thermal neutron counters, 9 – the pumping tube, 10 – the cooler tube, 11 – the valve of the He filling line, 12 – the tube of the high-vacuum line, 13 – the vacuum set-up chamber, 14 – copper stripes, 15 – the additional surface above the trap bottom and the entrance shutter, 16 – the entrance plane shutter, 17 – the pumping tube for the chamber bottom, 18 – the detector shutter, 19 – the UCN detector, 20 – a horizontal cross section of the set-up with blocks of polyethylene reflector for thermal neutrons.

inelastic scattering on the trap walls, was performed in 2008–2010 at the high-flux neutron reactor of Institut Max von Laue–Paul Langevin (ILL, Grenoble, France) [12]. Preliminary results, which accounted for some systematic corrections, were published earlier in conference proceedings [13,14]. In the present work, particular attention is devoted to analyzing all methodical effects of the method.

A scheme of the installation is shown in Fig. 1. A storage trap inside a double vacuum chamber, which is made of stainless steel, is shaped in a form of two vertical coaxial cylinders that are installed on a double flange. A coiled copper tube is entwined on the external surface of the internal cylinder in order to provide the circulation of liquid coolant, which is supplied from a closed cycle refrigerator. The bottom flange of the chamber has a cavity with the depth of 3.4 cm with a coiled cooling tube in it. This cavity is filled with a liquid fluorinated polymer so that the liquid covers the coiled tube.

A feed-through for the UCN guide tube is in the bottom flange. The upper plane of the guide tube is installed higher than the bottom flange by 5.5 cm. A plane UCN shutter could open and close the tube. The neutron guide system includes an input neutron guide with a UCN shutter; the guide is connected to a UCN source. The exit neutron guide is connected to a UCN detector with another shutter at its entrance. The UCN detector is a proportional gas counter filled with a gas mixture containing ^{3}He gas. The entrance window of the detector is an aluminum foil with the thickness of 100 μm and the diameter of 15 cm. The interior volume of the chamber is pumped on using a turbo molecular pump down to the residual gas pressure of 10^{-6}–10^{-5} mbar.

18 thermal neutron counters SNM-57 are fixed outside the chamber; these counters are located in two sections. This detector system measures neutrons, which are scattered inelastically on the walls of the storage trap. The detector shielding is made of cadmium and borated polyethylene; the shielding surrounds the whole set-up in order to suppress external neutron backgrounds.

Measurements are carried out in two geometries of the storage trap; these two options differ from each other by the frequency of UCN collisions with the trap walls arising due to different wall surface exposed to UCNs. In the geometry no. 1 UCNs are stored inside the copper cylindrical trap with the diameter of 40 cm and with the height of 95 cm. The bottom is covered with a thick layer of fluid fluorinated polymer; the internal surface of the copper cylinder is covered with a thin layer of such polymer. During the UCN filling interval, UCNs enter the trap through opened shutters (2), (3), as well as through the plane shutter (16), while the detector shutter (18) is closed. In order to restrict the energy of stored UCNs from above, the polyethylene disk with the diameter of 35 cm is installed on a fixed height H_d. After completion the time interval $t_{fill} = 150$ s, the plane shutter (16) and shutter (3) are closed while the detector shutter (18) is opened; thus the cleaning interval starts. During the cleaning interval lasting for $t_{clean} = 200$ s, the UCN energy spectrum is shaped. Then the polyethylene disk is moved to a height of $H_{max} = 95$ cm. After the polyethylene disk reaches H_{max}, the storage interval starts; it continues during the interval $t_1 = 60$ s. At the end of the storage interval, the plane shutter (16) is opened and stored UCNs flow down into the UCN detector during the detection interval $t_{reg} = 150$ s. Then the filling and cleaning intervals are repeated again, however the UCN storage interval is different $t_2 = 960$ s. The total UCN loss probability (per time unit) during the storage time interval, is calculated as follows: $\lambda_1 = \frac{1}{\tau_1} = \frac{1}{t_2 - t_1} \ln \frac{N_1(t_1)}{N_1(t_2)}$, where $N_1(t_1)$ and $N_1(t_2)$ are numbers of detected UCNs, τ_1 is the storage time. In the geometry no. 2, the surface area of the storage volume is increased by inserting 90 copper strips with a thickness of 100 μm and a width of 15 mm. In addition, a copper foil ring with the thickness of 100 μm is inserted at a height of 1.4 cm above the trap bottom; an analogous foil is inserted at the height of 1.5 cm above the plane shutter (16). The surfaces of all strips and both foils are covered with identical fluorinated polymer layers. As a result, the total surface exposed to UCNs increases by a factor of 3.

The intervals t_{fill}, t_{clean} and t_{reg} for the measurements in the geometry no. 1 are equal to those in the geometry no. 2, while the storage intervals for the measurements in geometry no. 2 are shorter by a factor of 3, and are equal accordingly to $t_1 = 20$ s and $t_2 = 320$ s. This shortening of the storage intervals is needed in order to provide equal total number of UCN collisions during the storage interval for the two geometries, with the purpose to keep identical UCN energy spectra. The total UCN loss probability (per time unit) during the storage interval is calculated for the geometry no. 2 as follows $\lambda_2 = \frac{1}{\tau_2} = \frac{1}{t_2 - t_1} \ln \frac{N_2(t_1)}{N_2(t_2)}$, where $N_2(t_1)$ and $N_2(t_2)$ are the numbers of detected UCNs, τ_2 is the storage time.

The total UCN loss probabilities (per time unit) are

$$\lambda_1 = \lambda_\beta + \lambda_{l1}, \qquad \lambda_2 = \lambda_\beta + \lambda_{l2}, \tag{1}$$

where λ_β, λ_{l1}, λ_{l2} are correspondingly the β-decay probability and the loss probabilities via neutron collisions with the walls for the two geometries. As far as the ratio $\xi = \frac{\lambda_{l2}}{\lambda_{l1}}$ is measured, the neutron β-decay probability is calculated as follows:

$$\lambda_\beta = \frac{\xi\lambda_1 - \lambda_2}{\xi - 1}. \tag{2}$$

The value of ξ could be measured using count rates in the thermal neutron detectors during the storage intervals t_1 and t_2. J_1 for the geometry no. 1 and J_2 for the geometry no. 2:

$$J_1 = \frac{N_1(t_1) - N_1(t_2)}{\lambda_1} \lambda_{l1} \frac{\varepsilon_{th1}\sigma_{ie}}{\varepsilon_{ucn1}(\sigma_{ie} + \sigma_c)}, \tag{3}$$

$$J_2 = \frac{N_2(t_1) - N_2(t_2)}{\lambda_2} \lambda_{l2} \frac{\varepsilon_{th2}\sigma_{ie}}{\varepsilon_{ucn2}(\sigma_{ie} + \sigma_c)}. \tag{4}$$

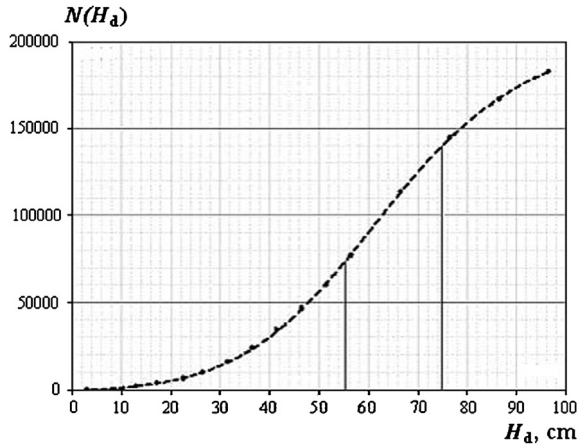

Fig. 2. The number of UCNs in the trap as a function of height H_d of the polyethylene disk.

Here ε_{ucn1} and ε_{ucn2} are the efficiencies of UCN detection for the geometries no. 1 and no. 2 respectively, ε_{th1} and ε_{th2} are analogous efficiencies of detection of neutrons inelastically scattered on the trap walls, σ_{ie} is the cross section of neutron inelastic scattering in the wall material, and σ_c is the cross section of neutron capture in the wall material.

If UCN numbers were defined correction-free, if the equalities $\varepsilon_{ucn1} = \varepsilon_{ucn2}$ and $\varepsilon_{th1} = \varepsilon_{th2}$ were precise, if no residual gas was present in the trap, if the temperatures of the main surface and that of the additional one were equal, then the ξ-value would be equal to

$$\xi = \xi_0 = \frac{J_2}{J_1}\frac{\lambda_2}{\lambda_1}\frac{N_1(t_1) - N_1(t_2)}{N_2(t_1) - N_2(t_2)}. \tag{5}$$

The neutron lifetime value defined in Eqs. (1), (2), (5) is called below "uncorrected".

2. The measurement results

Fig. 2 shows the number of UCNs in the trap as a function of the height H_d of the polyethylene disk. For each height H_d of the polyethylene disk in the geometry no. 1, the trap is filled in following a usual procedure. Most neutrons with the large enough maximum raising height in the gravitational field $H > H_d$ leave the trap during 200 s via their inelastic scattering in the disk material. The fraction of residual UCNs with the maximum raising height $H > H_d$ is smaller than (1–2)% by the end of the cleaning interval; at this moment UCNs are released to the UCN detector.

For the present neutron lifetime experiment, two options for the absorber height are used: $H_d = 55$ cm and $H_d = 75$ cm. The number of UCNs in the trap is equal respectively to $\approx 7.0 \cdot 10^4$ and $\approx 13.7 \cdot 10^4$. Small heating of UCNs [15–17] during the storage interval occurred with the probability of $1.3 \cdot 10^{-5}$ per one wall reflection and populated the neutron spectrum at heights $H > H_d$; the typical energy difference $(H - H_d)$ was lower than (15–20) cm. To decrease systematic effects resulting from this small UCN heating on UCN storage times, we raised up the polyethylene disk to the height of $H_{max} = 95$ cm when the storage interval starts.

As an example, the count rate in a detector of thermal neutrons $j(t)$ and the count rate in the UCN detector $j_{ucn}(t)$ are shown in Figs. 3 and 4 as a function of time for a measurement cycle in geometries 1 and 2 for the spectrum shaping height $H_d = 55$ cm and the temperature of 23 °C.

A series of n measuring cycles was performed for each geometry. A single measurement in geometry 1 provides two values $\lambda_1 = \frac{1}{\tau_1}$ and λ_{l1}. After multiple repetition of the measurements, the trap was open and the additional surface was inserted into it. Then measurements in geometry 2 were started. A single measurement in geometry 2 provides two values $\lambda_2 = \frac{1}{\tau_2}$ and λ_{l2}. Figs. 5, 6 and 7 show the scattering of measured values over different cycles, and also their mean values for different conditions of UCN storage. The statistical uncertainties of the measurements $\delta\lambda_1 = \frac{1}{t_2 - t_1}\sqrt{\frac{1}{N_1(t_1)} + \frac{1}{N_1(t_2)}}$, $\delta\lambda_2 = \frac{1}{t_2 - t_1}\sqrt{\frac{1}{N_2(t_1)} + \frac{1}{N_2(t_2)}}$, $\delta\tau_1 = \frac{\delta\lambda_1}{(\lambda_1)^2}$, $\delta\tau_2 = \frac{\delta\lambda_2}{(\lambda_2)^2}$ were calculated in the standard way. As the measurements are performed in each cycle with nearly equal statistical uncertainty, the mean values $\bar{\tau}_1$ and $\bar{\tau}_2$ are given with the uncertainties $\delta\bar{\tau}_1 = \frac{\delta\tau_1}{\sqrt{n}}$, $\delta\bar{\tau}_2 = \frac{\delta\tau_2}{\sqrt{n}}$, and also with the uncertainties defined by their deviation from the mean value $(\delta\tau)_{dev} = \sqrt{\sum_{i=1}^{n} \frac{(\tau_i - \bar{\tau})^2}{n(n-1)}}$, where $\bar{\tau} = \frac{1}{n}\sum_{i=1}^{n} \tau_i$, τ_i is the storage time in a single measurement.

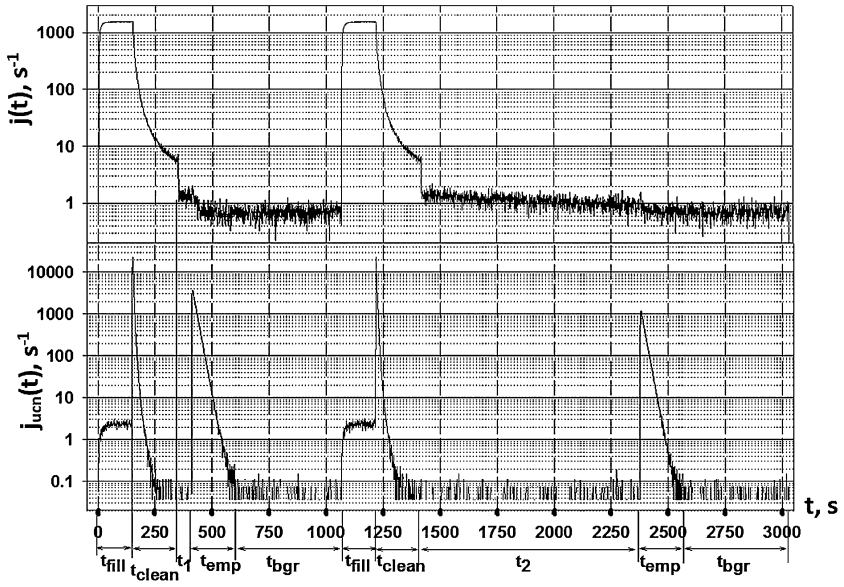

Fig. 3. The count rate in a detector of thermal neutrons $j(t)$ and the count rate in the UCN detector $j_{ucn}(t)$ are shown as a function of time for a measurement cycle in geometry 1 for the spectrum shaping height $H_d = 55$ cm and the temperature of 23 °C.

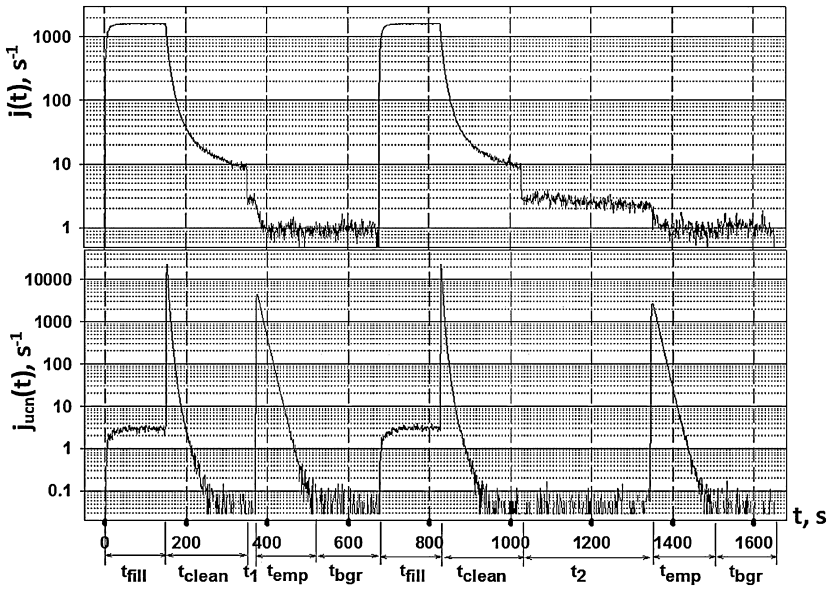

Fig. 4. The count rate in a detector of thermal neutrons $j(t)$ and the count rate in the UCN detector $j_{ucn}(t)$ are shown as a function of time for a measurement cycle in geometry 2 for the spectrum shaping height $H_d = 55$ cm and the temperature of 23 °C.

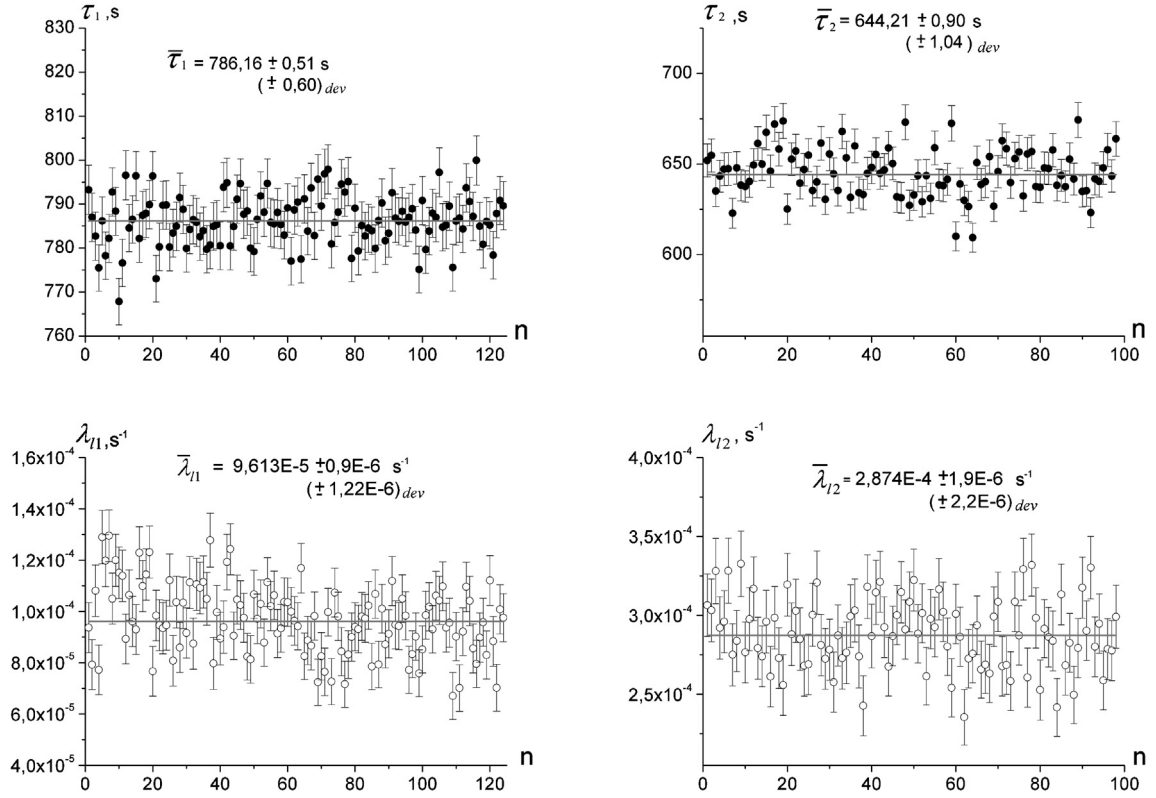

Fig. 5. Values τ_1, τ_2, λ_{l1}, λ_{l2} in consequent measuring cycles for geometries 1 and 2 for $H_d = 55$ cm, $t = +23$ °C, $\xi_0 = 2.99$.

Values $\lambda_{l1} = \frac{J_1\lambda_1\varepsilon_{ucn1}(\sigma_{ie}+\sigma_c)}{(N_1(t_1)-N_1(t_2))\varepsilon_{th1}\sigma_{ie}}$ and $\lambda_{l2} = \frac{J_2\lambda_2\varepsilon_{ucn2}(\sigma_{ie}+\sigma_c)}{(N_2(t_1)-N_2(t_2))\varepsilon_{th2}\sigma_{ie}}$ are given in relative units assuming also the equalities $\varepsilon_{ucn1} = \varepsilon_{ucn2}$ and $\varepsilon_{th1} = \varepsilon_{th2}$. Statistical uncertainties $\delta\lambda_{l1}$ and $\delta\lambda_{l2}$ of single measurements λ_{l1}, λ_{l2} were calculated in the standard way. Mean values $\bar{\lambda}_{l1}$ and $\bar{\lambda}_{l2}$ over cycles are given with uncertainties $\delta\bar{\lambda}_{l1} = \frac{\delta\lambda_{l1}}{\sqrt{n}}$, $\delta\bar{\lambda}_{l2} = \frac{\delta\lambda_{l2}}{\sqrt{n}}$, and also with uncertainties $(\delta\bar{\lambda}_{l1})_{dev}$ and $(\delta\bar{\lambda}_{l2})_{dev}$, calculated using their deviation from the mean value.

Small difference of the uncertainties obtained using the two methods is due to systematic effects, for instance, due to the variation of the incoming UCN flux during filling the trap in first exposition t_1 and that in second exposition t_2. Another reason for the difference in the values of uncertainties might consist of gradual drift in the value of the probability of UCN losses in wall collisions and thus the drifts of UCN storage times.

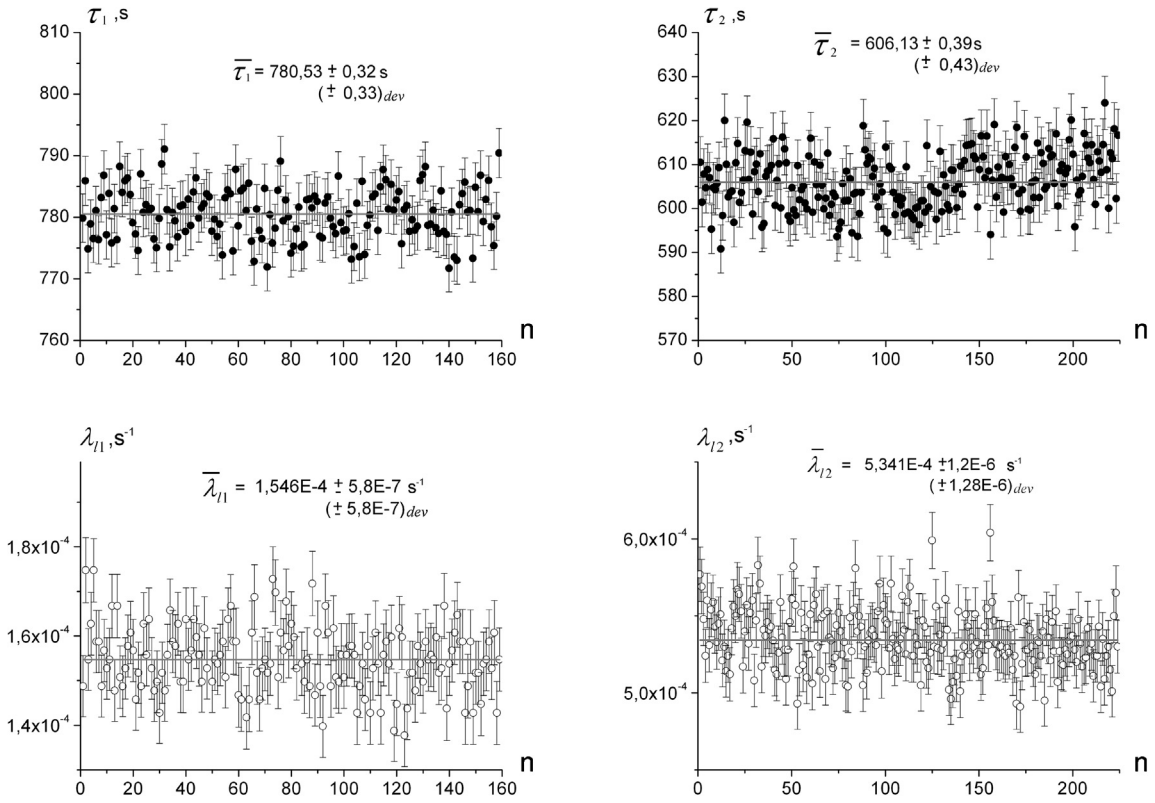

Fig. 6. Values τ_1, τ_2, λ_{l1}, λ_{l2} in consequent measuring cycles for geometries 1 and 2 for $H_d = 75$ cm, $t = +23\,^{\circ}$C, $\xi_0 = 3.454$.

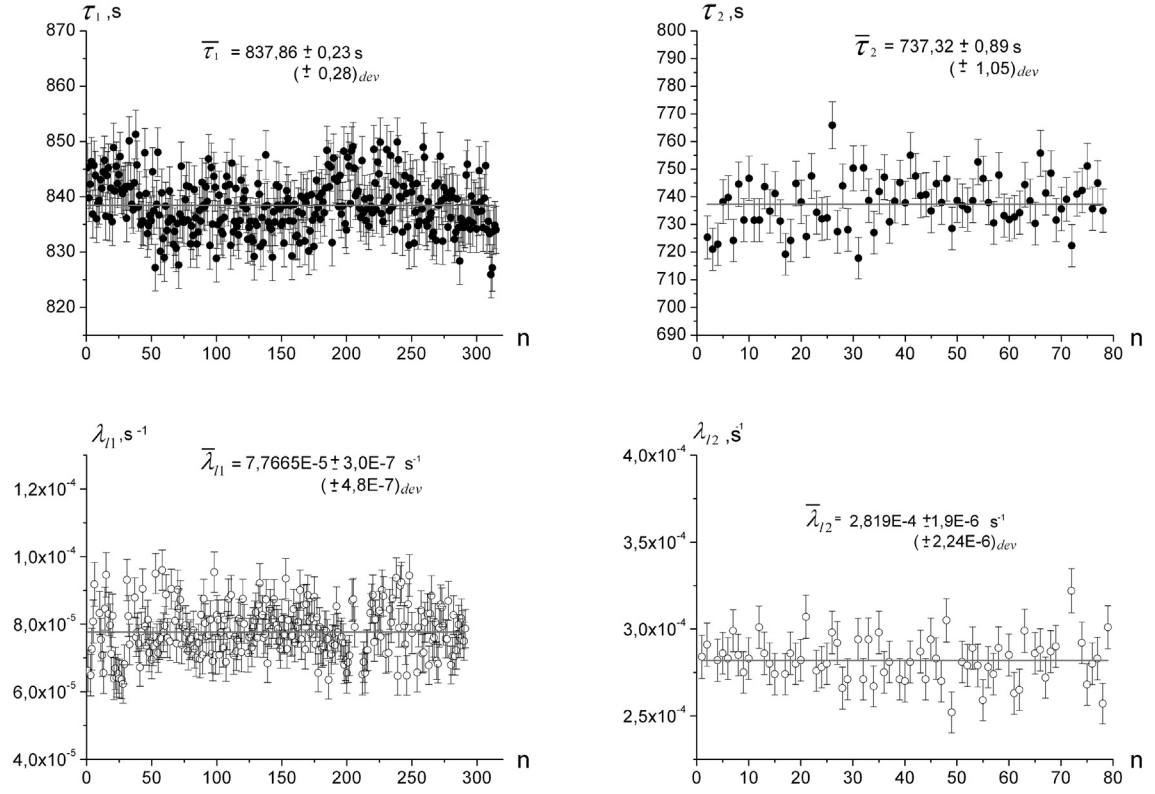

Fig. 7. Values τ_1, τ_2, λ_{l1}, λ_{l2} in consequent measuring cycles for geometries 1 and 2 for $H_d = 75$ cm, $t = -26\,^{\circ}$C, $\xi_0 = 3.629$.

In the following treatment of the data, we always use the maximum value of the two uncertainties for estimating the value τ_β.

We performed three independent neutron lifetime experiments under different experimental conditions (Table 1).

Table 1
Results of three independent neutron lifetime experiments performed under different experimental conditions.

H_d, cm	Temperature, °C	ξ_0	$\lambda_{l1}/\lambda_\beta$	$(\tau_\beta)_{\text{uncorrected}}$
55	+23	2.989	0.120	$884.15 \pm 2.10_{st}$
75	+23	3.454	0.127	$884.30 \pm 0.95_{st}$
75	−26	3.629	0.054	$883.60 \pm 0.95_{st}$

Note that when hypothetically using the alternative method of calculations of ξ_0 (instead of measuring this value experimentally using the flux of up-scattered neutrons), this value in all three experiments would be equal $\xi_0 = 3.0$. Then the data shown in Figs. 5, 6, 7 would provide the following uncorrected values:

$\tau_\beta = 883.50$ s for $H_d = 55$ cm, $t = +23\,^\circ$C;

$\tau_\beta = 911.69$ s for $H_d = 75$ cm, $t = +23\,^\circ$C;

$\tau_\beta = 899.20$ s for $H_d = 75$ cm, $t = -26\,^\circ$C.

Evidently, the values τ_β would scatter by 10–25 s that is significantly larger than the corresponding uncertainties. This scattering indicates that there are systematic errors in the method of calculations of ξ_0, which are caused by eventual difference of coefficients μ_1 and μ_2 of UCN losses in trap walls in two geometries, or by eventual deviation of mean frequencies of collisions p_1 and p_2 from calculated values.

3. Systematic corrections

The main systematic correction arises from the partial loss of count rate in the UCN detector (dead-time correction); it shifts the values of probabilities λ_{l1}, λ_{l2} as well as the value of ξ_0. Other corrections are introduced via calculating the value $\xi = \xi_0 + \Delta\xi$, where $\Delta\xi$ is a systematic correction, which meets the following equation for the corrected value of the neutron lifetime τ_β: $\frac{\Delta\lambda_\beta}{\lambda_\beta} = \frac{\lambda_{l1}}{\lambda_\beta}\frac{\xi}{\xi-1}\frac{\Delta\xi}{\xi}$. A corresponding neutron lifetime τ_β-correction is $(\Delta\tau_\beta) = -\tau_\beta\frac{\Delta\lambda_\beta}{\lambda_\beta}$, where τ_β-value is assumed to be equal to the world mean weighted value 880.0 s. One should note that a small (<1%) uncertainty in the chosen value of τ_β does not affect the systematic corrections $(\Delta\tau_\beta)$ because their relative uncertainties are defined less precisely (see Table 2). Thus, if $\Delta\xi > 0$ then $\Delta\tau_\beta < 0$, and on contrary, if $\Delta\xi < 0$ then $\Delta\tau_\beta > 0$.

3.1. A correction caused by a partial loss of the count rate in the UCN detector

UCNs were measured in a gaseous proportional detector with a pre-amplifier and with an amplifier-shaper (Fig. 8); pulses with the maximum amplitude of 3 V and the duration of 2.5 μs were shaped at its exit. Analogous pulses were sent to a discriminator with the window $U_L = 1.0$ V, $U_{UP} = 9.0$ V. As soon as an analogous pulse fitted into the window, a pulse with the duration 0.5 μs was produced. These pulses were sent to a counter, which measured them with the rate J_m.

The actual rate of neutron detection is $J = J_m + J_m J\tau_d$, where τ_d is the dead-time of the detection system. Losses in the count rate caused by the dead-time of the detection system were investigated using the flux of UCNs, which is controlled by valves 2, 3, 18 (Fig. 1). The count rate J_m was measured during the interval (1000–20 000) s^{-1}. For a given value J_m, pulses from the discriminator were sent to the time analyzer, which measured the time of their arrival t_i. A measured sequence of pulses (events) was recorded in a PC, and the number of events was summed up over the interval t as follows. Sum N included an initial event t_1, however further events in the interval $t_1 + T_d$ (Fig. 8) were not included. The following event t_2, happened after expiration of time $t_1 + T_d$ was included, however events during $t_2 + T_d$ were not included. This algorithm provided the sum of events $N(T_d)$ detected during interval from 0 to t, and the count rate $J_m(T_d) = \frac{N(T_d)}{t}$. Fig. 9 shows the dependence $\frac{1}{J_m(T_d)} = \frac{1}{J} + \tau_d$, calculated from treating a sequence of pulses from the discriminator arriving with the frequency $J_m \approx 5 \cdot 10^3$ s^{-1}. As clear from the figure, as soon as $T_d \le \tau_d$ the value $J_m(T_d)$ does not change. A linear extrapolation of the count rate towards $T_d = 0$ allows estimating the actual rate J and the dead-time of the detection system $\tau_d = 2.7$ μs.

Analogous dependencies were measured for other values J_m. The dead time τ_d of the electronic units is measured for the frequency of pulses J_m in the range of 1000–20 000 s^{-1}, it is equal to $\tau_d = (2.7 \pm 0.1) \cdot 10^{-6}$ s (Fig. 10).

During the detection interval, the measured count rate in the UCN detector rises up to the value of $\sim 10^4$ s^{-1}, then it decreases exponentially down with a typical emptying time constant of (11–14) s (Fig. 4). The loss in the count rate is caused by a non-zero dead time τ_d of the electronic units. The true value of the count rate would be equal to $J = J_m(1 + J_m\tau_d)$. All measured values of $N_1(t_1)$, $N_1(t_2)$, $N_2(t_1)$, $N_2(t_2)$ are corrected, then the corrected values of λ_{l1}, λ_{l2} and ξ_0 are used to calculate the corrected value of τ_β.

Fig. 11 shows the absolute shift $(\Delta\tau_\beta)_d$ in the neutron lifetime value as a function of the dead time τ_d. This shift is of negative sign; or the corrected value of τ_d is lower than the uncorrected one.

Data in Fig. 11 are used to calculate the correction $(\Delta\tau_\beta)_d$ and its uncertainty; the results are given in Table 2.

We introduced analogous corrections also in measurements [4,18]; however dead-time in those works was estimated using the

Table 2
The systematic corrections estimated above.

The reason for correction	Time [s]		
	$H_d = 55$ cm, $T = +23\,^\circ$C	$H_d = 75$ cm, $T = +23\,^\circ$C	$H_d = 75$ cm, $T = -26\,^\circ$C
Uncorrected τ_β-values	$884.15 \pm 2.10_{stat}$	$884.30 \pm 0.95_{stat}$	$883.60 \pm 0.95_{stat}$
Partial count rate loss in the UCN detector	-1.28 ± 0.15	-3.01 ± 0.18	-3.82 ± 0.14
Scattering of UCN on residual gas	-1.84 ± 0.31	-0.43 ± 0.12	0.17 ± 0.10
Difference in ε_{ucn1} and ε_{ucn2}	-0.61 ± 0.11	-0.23 ± 0.06	-0.24 ± 0.03
Difference in $\varepsilon_{ucn}^{(i)}$ and $\varepsilon_{ucn}^{(f)}$	-0.15 ± 0.06	0.0 ± 0.06	0.0 ± 0.06
Difference in ε_{th1} and ε_{th2}	1.00 ± 0.40	0.46 ± 0.24	0.18 ± 0.09
Difference in temperatures in the geometries 1 and 2	No correction	No correction	0.11 ± 0.06
Eventual leak through the trap UCN shutter	0 ± 0.05	0 ± 0.05	0 ± 0.05
The cross section ratios inequality	0 ± 0.03	0 ± 0.03	0 ± 0.01
Weak heating	-0.38 ± 0.38	-0.52 ± 0.52	-0.03 ± 0.03
Leakage of ^{3}He into the trap volume	<0.01	<0.01	<0.01
The total systematic correction	-3.26 ± 1.49	-3.73 ± 1.26	-3.63 ± 0.57
τ_β-values with all systematic corrections	880.89 ± 3.59	880.57 ± 2.21	879.97 ± 1.52

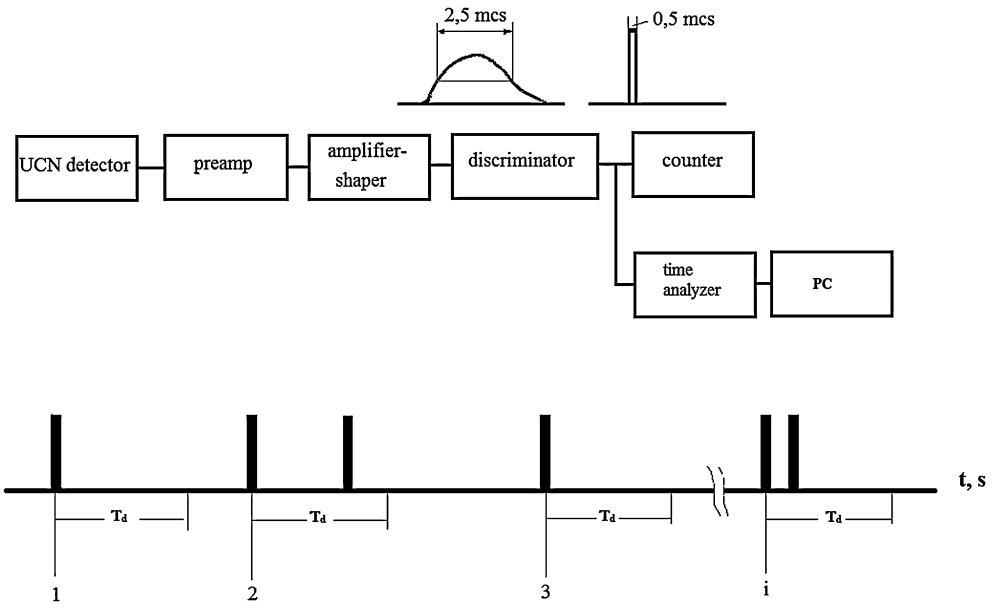

Fig. 8. A scheme of UCN detection and the estimation of the "dead-time" of the detection system τ_d.

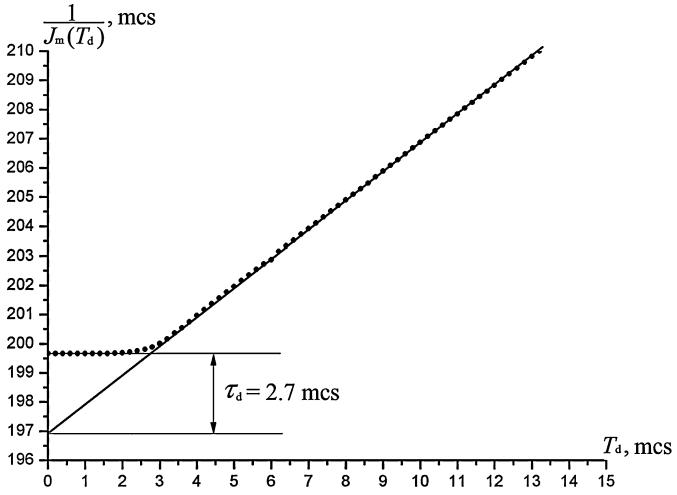

Fig. 9. A dependence $\frac{1}{J_m(T_d)} = \frac{1}{J} + \tau_d$ for $J_m \approx 5 \cdot 10^3$ s^{-1}.

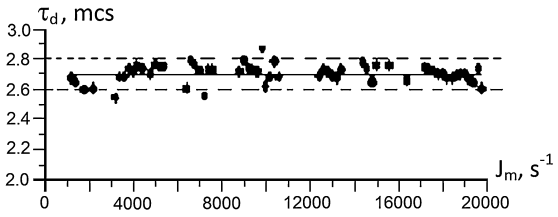

Fig. 10. Estimation of the τ_d-value as a function of the frequency J_m of pulses in the UCN detector.

method of dividing the detector into sections and detecting UCNs. A correction for dead-time was introduced into measured values $N_1(t_1)$, $N_1(t_2)$, $N_2(t_1)$, $N_2(t_2)$, and an uncertainty of estimating the dead-time was included into the statistical uncertainty.

3.2. A correction caused by residual gas inside the trap

Residual gas molecules are a source of additional scattering and capture of UCNs during the storage interval. The loss probabilities are then equal to

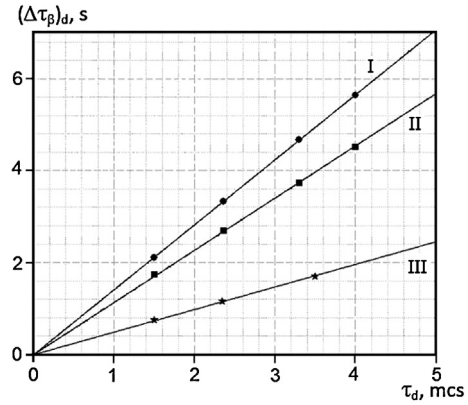

Fig. 11. The absolute shift $(\Delta\tau_\beta)_d$ in the neutron lifetime value as a function of the dead time τ_d for I – $H = 75$ cm, $t = -26\,^\circ$C; II – $H = 75$ cm, $t = 23\,^\circ$C; III – $H = 55$ cm, $t = 23\,^\circ$C.

$$\lambda_1 = \lambda_\beta + \lambda_{l1} + \lambda_{g1} = \lambda_\beta + \lambda^*_{l1} \quad \text{and}$$

$$\lambda_2 = \lambda_\beta + \lambda_{l2} + \lambda_{g2} = \lambda_\beta + \lambda^*_{l2},$$

where λ_{g1} and λ_{g2} are the probabilities of loss of UCNs in their interaction with the gas molecules. In this case, instead of Eq. (2) we have to use another expression:

$$\xi^* = \frac{\lambda^*_{l2}}{\lambda^*_{l1}} = \frac{\lambda_{l2} + \lambda_{g2}}{\lambda_{l1} + \lambda_{g1}}. \tag{6}$$

The experimental value of ξ_0 in presence of residual gas inside the storage trap is equal $\xi_0 = \frac{J_2\lambda_2}{N_2(0)-N_2(t_2)} \frac{N_1(0)-N_1(t_1)}{J_1\lambda_1} = \frac{\alpha\lambda_{l2}+\beta\lambda_{g2}}{\alpha\lambda_{l1}+\beta\lambda_{g1}} = \frac{\lambda_{l2}+\frac{\beta}{\alpha}\lambda_{g2}}{\lambda_{l1}+\frac{\beta}{\alpha}\lambda_{g1}}$, where coefficients α and β are equal to: $\alpha = \frac{\varepsilon_{th}\sigma_{ie}}{\varepsilon_{ucn}(\sigma_{ie}+\sigma_c)}$, $\beta = \frac{\varepsilon^*_{th}\sigma^*_{ie}}{\varepsilon_{ucn}(\sigma^*_{ie}+\sigma^*_c)}$.

Here ε^*_{th} and σ^*_{ie} are the efficiencies of detection of neutrons up-scattered on residual gas molecules and the cross section of neutron inelastic scattering on gas molecules respectively, and σ^*_c

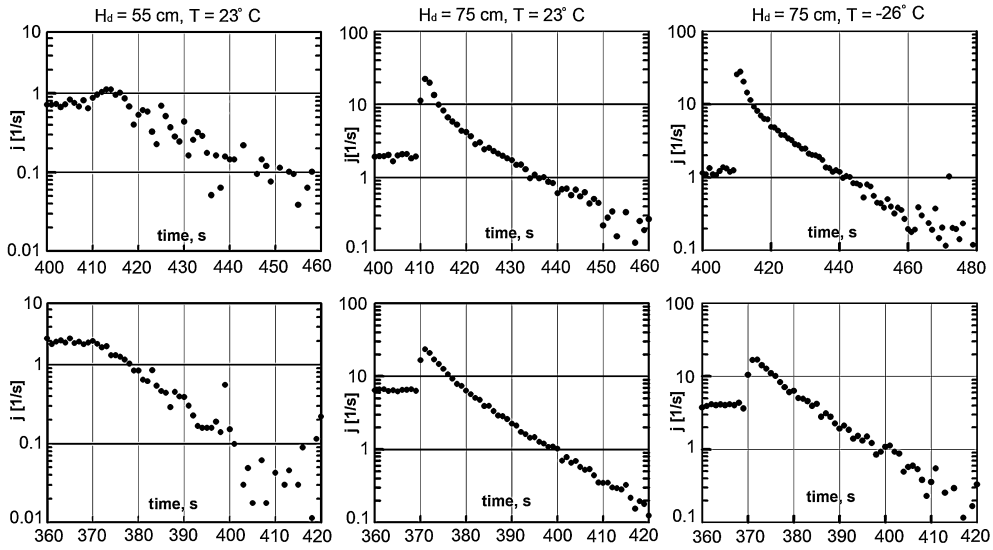

Fig. 12. Evolution of the count rate $j(t)$ in the thermal neutron detector during the emptying interval after the first UCN storage interval; this count rate serves to calculate the values N_i.

is the cross section of neutron capture in nuclei of residual gas molecules.

The shift in the $\Delta\xi^*$-value, with $\Delta\xi^* = \xi^* - \xi_0$, is:

$$\Delta\xi^* = \frac{\lambda_{l2}+\lambda_{g2}}{\lambda_{l1}+\lambda_{g1}} - \frac{\lambda_{l2}+\frac{\beta}{\alpha}\lambda_{g2}}{\lambda_{l2}+\frac{\beta}{\alpha}\lambda_{g2}} = -\frac{(\frac{\beta}{\alpha}-1)(\lambda_{g2}\lambda_{l1}-\lambda_{g1}\lambda_{l2})}{(\lambda_{l1}+\frac{\beta}{\alpha}\lambda_{g1})(\lambda_{l1}+\lambda_{g1})}. \quad (7)$$

The probabilities λ_{g1} and λ_{g2} are calculated using the measured values of the gas pressure P and the typical values $P\tau$ of the residual gas in the trap. The ratios $\frac{\beta}{\alpha}$ are measured experimentally; they are equal to: $\frac{\beta}{\alpha} = 1.518 \pm 0.075$ for $H_d = 55$ cm and $T = +23\,^\circ$C; $\frac{\beta}{\alpha} = 1.36 \pm 0.07$ for $H_d = 75$ cm, $T = +23\,^\circ$C, and $\frac{\beta}{\alpha} = 0.711 \pm 0.130$ for $H_d = 75$ cm, $T = -26\,^\circ$C. The correction values $(\Delta\tau_\beta)_g$ are listed in Table 2.

3.3. A correction caused by the difference in the UCN detection efficiencies in the geometries no. 1 (ε_{ucn1}) and no. 2 (ε_{ucn2})

This difference in the UCN detection efficiencies arises because of different values of the UCN emptying and storing times in measurements in the geometries no. 1 (ε_{ucn1}) and no. 2 (ε_{ucn2}). Moreover, the output shutter (16 in Fig. 1) during its opening moves up with the velocity of 30–40 cm/s and thus UCNs reflected from the shutter upside increased their velocity. When the UCN spectrum is shaped at the height of $H_d = 75$ cm, these reflected UCNs raise to the polyethylene disk at the height of ($H_{max} = 95$ cm) and leave the storage trap after inelastic scattering or capture inside the disk.

Fig. 12 shows the evolution of the count rate $j(t)$ in the thermal neutron detector, which corresponds to measuring the value N_i, during the emptying interval after the first UCN storage interval. If $H_d = 55$ cm in both geometries, this dependence has a smooth exponential shape as inelastic scattering of UCNs occurs only at the surfaces covered with Fluorine polymer. However, if $H_d = 75$ cm in both geometries, a raise in the $j(t)$ values occurs at the moment of shutter opening; then the flux evolves gradually into the exponential shape. This feature means that, in this case, the UCN inelastic scattering occurs during emptying not only at the surfaces covered with Fluorine polymer but also in the polyethylene disk ($H_{max} = 95$ cm).

The data shown in Fig. 12 allow estimating experimentally the corresponding correction $(\Delta\tau_\beta)_{ucn}$, which results from the inequality $\varepsilon_{ucn1} \neq \varepsilon_{ucn2}$. The systematic correction is defined as follows $\frac{\Delta\xi}{\xi} = \frac{\varepsilon_{ucn2}-\varepsilon_{ucn1}}{\varepsilon_{ucn1}}$, where

$$\frac{\varepsilon_{ucn2}-\varepsilon_{ucn1}}{\varepsilon_{ucn1}} = \frac{[\frac{\varepsilon_{ucn1}(\sigma_{ie}+\sigma_c)}{\varepsilon_{th1}\sigma_{ie}N_{i1}}\int_0^{t_{reg}} j_1(t)dt - \frac{\varepsilon_{ucn2}(\sigma_{ie}+\sigma_c)}{\varepsilon_{th2}\sigma_{ie}N_{i2}}\int_0^{t_{reg}} j_2(t)dt] - [\frac{\lambda_\beta}{\lambda_{emp2}} - \frac{\lambda_\beta}{\lambda_{emp1}}]}{1 - \frac{\varepsilon_{ucn1}(\sigma_{ie}+\sigma_c)}{\varepsilon_{th1}\sigma_{ie}N_{i2}}\int_0^{t_{reg}} j_1(t)dt - \frac{\lambda_\beta}{\lambda_{emp1}}}. \quad (8)$$

Here $t_{reg} = 150$ s is the interval of counting UCNs in the UCN detector after their emptying from the storage trap, N_{i1} N_{i2} are the numbers of UCNs measured after the first filling interval in the geometries 1 and 2 respectively, $\lambda_{emp1} = \frac{1}{\tau_{emp1}}$ and $\lambda_{emp2} = \frac{1}{\tau_{emp2}}$ are the probabilities of counting UCNs in the detector, τ_{emp1} and τ_{emp2} are the corresponding emptying times. Dimensionless expressions $\frac{\varepsilon_{ucn1}(\sigma_{ie}+\sigma_c)}{\varepsilon_{th1}\sigma_{ie}}$ and $\frac{\varepsilon_{ucn2}(\sigma_{ie}+\sigma_c)}{\varepsilon_{th2}\sigma_{ie}}$ were calculated using Eq. (3) and Eq. (4) basing on the UCN storage data and the data shown in Fig. 12. The corresponding correction value $(\Delta\tau_\beta)_{ucn}$ could be found in Table 2.

3.4. A correction caused by the difference in the UCN detection efficiencies at the initial $\varepsilon_{ucn}^{(i)}$ and final $\varepsilon_{ucn}^{(f)}$ moments of the UCN storage

This difference could arise if the corresponding UCN energy spectra are different at initial t_1 and final t_2 time moments. Due to small UCN heating, the initial UCN energy spectrum during the storing interval is enriched with neutrons with the energy higher than the initial maximum energy shaped at the disk height H_d. On the other hand, the spectrum is depleted from UCNs with high energy due to the energy-dependent rate of UCN losses in the walls. The relative difference in the efficiencies is defined as follows

$$\frac{\varepsilon_{ucn}^{(i)}-\varepsilon_{ucn}^{(f)}}{\varepsilon_{ucn}^{(i)}} = \frac{\frac{\varepsilon_{ucn}(\sigma_{ie}+\sigma_c)}{\varepsilon_{th}\sigma_{ie}}[\frac{1}{N_f}\int_0^{t_{reg}} j_f(t)dt - \frac{1}{N_i}\int_0^{t_{reg}} j_i(t)dt] - [\frac{\lambda_\beta}{\lambda_{emp(i)}} - \frac{\lambda_\beta}{\lambda_{emp(f)}}]}{1 - \frac{\varepsilon_{ucn}(\sigma_{ie}+\sigma_c)}{\varepsilon_{th}\sigma_{ie}N_i}\int_0^{t_{reg}} j_i(t)dt - \frac{\lambda_\beta}{\lambda_{emp(i)}}} \quad (9)$$

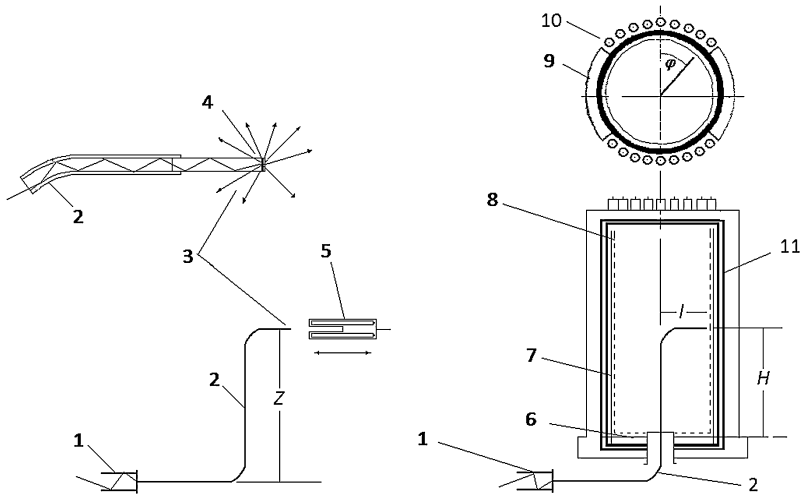

Fig. 13. A scheme of calibrating the source of thermal neutrons and a method of measuring the difference $\frac{\Delta\varepsilon_{th}}{\varepsilon_{th2}} = \frac{\varepsilon_{th2}-\varepsilon_{th1}}{\varepsilon_{th2}}$ in the detection efficiencies. 1 – the neutron guide from the UCN source; 2 – the flexible neutron guide made of polyvinyl chloride; 3 – the movable source of thermal neutrons; 4 – the polyethylene disk; 5 – the thermal neutron detector (monitor); 6 – the bottom of the storage trap (a layer of fluorine polymer YH VAC 18/8); 7 – the cylindrical surface (wall) of the trap; 8 – the additional surface (dotted line); 9 – the reflector made of polyethylene; 10 – SNM-57 counters (18 pieces); 11 – the vacuum chamber.

where N_i and N_f are the numbers of UCNs measured after the first and second counting intervals, $j_i(t)$ and $j_f(t)$ are the count rates in the thermal neutron detector during the corresponding emptying intervals, $\lambda_{emp(i)} = \frac{1}{\tau_{emp(i)}}$ and $\lambda_{emp(f)} = \frac{1}{\tau_{emp(f)}}$ are the probabilities of the UCN counting in the detector, $\tau_{emp(i)}$ and $\tau_{emp(f)}$ are the corresponding emptying times. Using Eq. (9), we estimated the value $\frac{\varepsilon^{(i)}_{ucn}-\varepsilon^{(f)}_{ucn}}{\varepsilon^{(i)}_{ucn}}$ for three measurement series and the corresponding correction values $(\Delta\tau_\beta)_{i-f}$ are given in Table 2.

3.5. A correction caused by the difference in the detection efficiencies of the inelastically scattered neutrons in the thermal neutron detectors in the geometries no. 1 (ε_{th1}) and no. 2 (ε_{th2})

A small difference in the detection efficiencies is caused by two factors. First, it is due to different positions of the surfaces that emit inelastically scattered neutrons with respect to the external detector in different geometries. Second, it is due to additional scattering and capture of scattered neutrons in the matter (copper) of the additional surfaces in the geometry 2.

For evaluating experimentally the corresponding correction $\frac{\Delta\xi_{th}}{\xi} = -\frac{\varepsilon_{th2}-\varepsilon_{th1}}{\varepsilon_{th2}}$, we used a special movable tiny source of thermal neutrons (see Fig. 13) [19,20]. A flexible polyvinyl chloride tube with the internal diameter of 8 mm was connected to the UCN source. A copper cylinder with thin walls and a piece of polyethylene (target) with the thickness of 0.2 mm was connected to the end of the tube. UCNs passing through the tube hit the target, which convert UCNs into thermal neutrons with isotropic angular distribution and the mean energy of 0.015 eV. The intensity of this source of thermal neutrons is measured using a monitor detector. The intensity changes as a function of the source height $Z = (0\text{–}100)$ cm in the range of $(300\text{–}50)$ s^{-1}.

If the source is introduced inside the storage trap and placed close to its surface in the geometry 1, we measured that the count rate in the thermal neutron detector changes as a function of the source position ($l = 20$ cm, φ, H). Fig. 14 shows the average (over the angle φ, and the height H above the bottom) value of the detection efficiency of thermal neutrons emitted by the source.

Then the additional surface is introduced into the trap, and the dependence of the count rate in the detector is measured another time as a function of the source position; the source is placed close to the surface of the trap in the geometry 1, also the source is placed close to the additional surface of the trap (the geometry 2). Using the measured data, also taking into account the heterogeneity of emitted inelastically scattered neutrons due to the gravitational field, the shift in $\frac{\Delta\varepsilon_{ih}}{\varepsilon_{ih2}}$-value is evaluated for the two stored UCN spectra: $\frac{\Delta\varepsilon_{ih}}{\varepsilon_{ih2}} = 0.0062 \pm 0.0025$ for $H_d = 55$ cm and $\frac{\Delta\varepsilon_{ih}}{\varepsilon_{ih2}} = 0.0029 \pm 0.0015$ for $H_d = 75$ cm. The corresponding systematic correction to the neutron lifetime value $(\Delta\tau_\beta)_{ih}$, estimated using these results, is given in Table 2.

3.6. A correction caused by the difference in temperatures of the storage trap in the geometries 1 and 2

This correction is caused by the difference in mean temperatures for the geometry no. 1 ($T_1 = -(27.2 \pm 0.5)\,^\circ$C) and for the geometry no. 2 ($T_2 = T_1 + \Delta T = -(25.8 \pm 0.5)\,^\circ$C), where the ΔT-difference is equal to $(1.4 \pm 0.7)\,^\circ$C, and the correction is $\frac{\Delta\xi_T}{\xi_0} = 1\frac{1+\frac{\sigma_c}{\sigma_{ie}(T_1)}}{1+\frac{\sigma_c}{\sigma_{ie}(T_1)+\frac{\partial\sigma_{ie}}{\partial T}\Delta T}}$. For these temperatures, the gradient of the neutron inelastic scattering cross section for fluid fluorine polymer is equal to $\frac{\partial\sigma_{ie}}{\partial T} = (1.483 \pm 0.068)$ barn/grad. The corresponding systematic correction for the neutron lifetime value is equal to $(\Delta\tau_\beta)_T = (0.11 \pm 0.06)$ s; the result is given in Table 2.

3.7. A correction caused by eventual UCN leaking through the UCN shutter of the storage trap

An eventual UCN leaking from the trap was measured experimentally as a difference between the count rate in the UCN detector during the storage interval and the background. Such a leak was absent (Table 2).

3.8. A correction for an eventual inequality of the cross section ratios in the geometries 1 and 2: $(\frac{\sigma_{ie}}{\sigma_{ie}+\sigma_c})_1$ and $(\frac{\sigma_{ie}}{\sigma_{ie}+\sigma_c})_2$

This correction could arise if the main surface and the additional surface were partly un-covered with fluorine polymer. Analysis of the experimental values of the storage time measured in the two geometries showed that the storage time values were close to the calculated ones for fluorine polymer, thus the ratio of naked copper areas is not higher than (0.5)%. The ratio of the cross sections $(\frac{\sigma_{ie}}{\sigma_{ie}+\sigma_c})$ at the ambient temperature is equal to

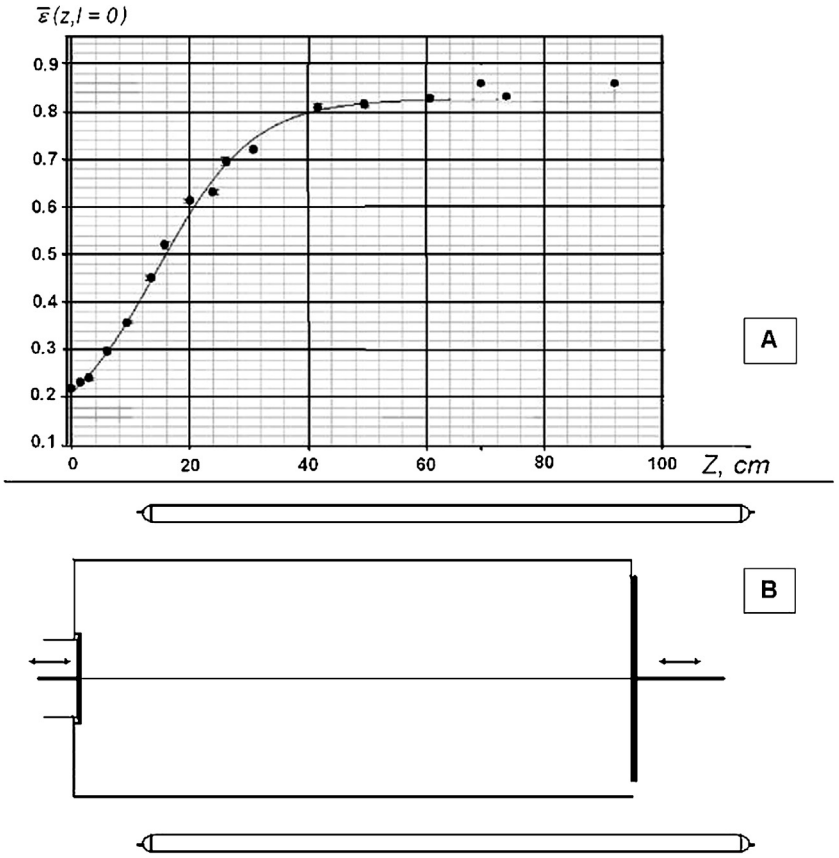

Fig. 14. A. The mean value of the detection efficiency $\boldsymbol{\varepsilon}$ for thermal neutrons emitted from the source (in relative units, averaged over the angle φ) as a function of height $\boldsymbol{Z}$ above the trap bottom. B. The vertical cross section of the storage trap and the system of thermal neutron detectors positioned horizontally.

$(\frac{\sigma_{ie}}{\sigma_{ie}+\sigma_c})_F = 0.95$ for the fluorine polymer while for copper it is equal to $(\frac{\sigma_{ie}}{\sigma_{ie}+\sigma_c})_{Cu} = 0.91$, the last value is defined by a hydrogen layer on the copper surface [21]. The correction that could be caused by eventual holes in the Fluorine polymer surface layer is estimated as follows

$$\frac{\Delta\xi_{ratio}}{\xi_0} = \pm\frac{\Delta(\frac{\sigma_{ie}}{(\sigma_{ie}+\sigma_c)})}{(\frac{\sigma_{ie}}{(\sigma_{ie}+\sigma_c)})_1} = \pm 1.8\times 10^{-4}. \quad (10)$$

This correction for the neutron lifetime value τ_β is estimated to be negligible (Table 2).

3.9. A correction caused by the presence of a weak UCN heating during storage

A major fraction of UCNs rises after weak heating to a height of not higher than (20–30) cm above the maximum height in the initial spectrum. However, a small fraction of UCNs could reach, after the weak heating, the polyethylene disk located at a height $H_{max} =$ 95 cm and thus inelastically scatter in it [22]. Such neutrons were detected with efficiency larger than the efficiency of detection of neutrons inelastically scattered in the trap walls (Fig. 14). This resulted in an additional difference in the detection efficiency for the two geometries of the experiment $(\frac{\Delta\varepsilon_{th}}{\varepsilon_{th2}})_{wh} = (\frac{\varepsilon_{th2}-\varepsilon_{th1}}{\varepsilon_{th2}})_{wh}$. This difference was calculated numerically [23] using the data [22] on the spectral energy change after weak heating of UCN. The total probability of weak UCN heating per collision was assumed to be equal to $1.3\cdot 10^{-5}$ at the temperature of $T = 23\,^\circ$C and equal $0.65\cdot 10^{-6}$ at the trap temperature of $T = -26\,^\circ$C. Corresponding corrections to the neutron lifetime value are presented in Table 2.

3.10. A correction caused by eventual leakage of ^{3}He from the UCN detector through the detector window to the trap volume

The correction caused by this effect is estimated experimentally by means of monitoring the evolution of efficiency of the UCN detector associated with eventual leakage of ^{3}He from the detector to the trap volume. The value of this correction to the neutron lifetime τ_β is estimated to be negligible (Table 2).

4. Conclusion

A resulting systematic correction in each column in Table 2 is evaluated by means of linear summing of all partial corrections and their uncertainties. Linear summation of uncertainties provides a very conservative upper estimation for the methodical uncertainty. Such a procedure is applied because we do not exclude that some methodical corrections could be correlated, and we are not sure that all possible correlations could be taken into account reliably. We thus obtained three independent results of measurements of the value τ_β in one setup at different experimental conditions of UCN storage with significantly different methodical corrections. The obtained results are self-consistent and are:

$$H_d = 55\text{ cm},\ t = +23\,^\circ\text{C};\quad \tau_\beta = 880.89 \pm 2.10_{\text{st}} \pm 1.49_{\text{meth}}\text{ s}$$

$$H_d = 75\text{ cm},\ t = +23\,^\circ\text{C};\quad \tau_\beta = 880.57 \pm 0.95_{\text{st}} \pm 1.26_{\text{meth}}\text{ s}$$

$$H_d = 75\text{ cm},\ t = -26\,^\circ\text{C};\quad \tau_\beta = 879.97 \pm 0.95_{\text{st}} \pm 0.57_{\text{meth}}\text{ s}$$

For averaging and calculating a final result we linearly add a statistical uncertainty and a methodical uncertainty in each measurement in order to get a single uncertainty of each measurement.

Thus we can estimate a mean value over three measurements. The last line in the Table 2 presents three independent results for the neutron lifetime τ_β-value. The result of measuring τ_β-value averaged over three independent results in the last line in Table 2 is equal to $\tau_\beta = (880.2 \pm 1.2)$ s.

This value agrees with results of other works based on the method of storage of UCNs [4–8] and included by Particle Data Grope in their analysis concerning the world average value [3]. However, our present result as well as all the data [4–8] is noticeably different from the results measured using the beam method [9–11].

Acknowledgements

The authors are grateful to the staff of the reactor ILL for their help during the measurements.

References

[1] D. Dubbers, M. Schmidt, Rev. Mod. Phys. 83 (2011) 1111.
[2] F.E. Wietfeldt, G.L. Green, Rev. Mod. Phys. 83 (2011) 1173.
[3] K.A. Olive, et al., Chin. Phys. C 38 (2014) 090001, http://pdg.lbl.gov.
[4] S.S. Arzumanov, et al., JETP Lett. 95 (2012) 224.
[5] W. Mampe, et al., JETP Lett. 57 (1993) 82.
[6] A. Serebrov, et al., Phys. Lett. B 605 (2005) 72;
A. Serebrov, et al., Phys. Rev. C 78 (2008) 035505.
[7] A. Pichlmaier, et al., Phys. Rev. B 693 (2010) 221.
[8] A. Steyerl, et al., Phys. Rev. C 85 (2012) 065503.
[9] J. Byrne, et al., Euro. Phys. Lett. B 605 (2005) 72.
[10] J.S. Nico, et al., Phys. Rev. C 71 (2005) 055502.
[11] A.T. Yue, et al., Phys. Rev. Lett. 111 (2013) 222501.
[12] S. Arzumanov, et al., Nucl. Instrum. Methods, Sect. A 611 (2009) 186.
[13] S. Arzumanov, et al., in: ISINN-17, Dubna, 2010, p. 355.
[14] S. Arzumanov, et al., in: ISINN-18, Dubna, 2011, p. 11.
[15] V.V. Nesvizhevsky, et al., Eur. Phys. J. Appl. Phys. 6 (1999) 151.
[16] L. Bondarenko, et al., Phys. At. Nucl. 65 (2002) 11.
[17] V.V. Nesvizhevsky, et al., New J. Phys. 14 (2012) 093053.
[18] S. Arzumanov, et al., Phys. Lett. B 483 (2000) 15;
S. Arzumanov, et al., Nucl. Instrum. Methods, Sect. A 440 (2000) 511.
[19] S.S. Arzumanov, et al., Crystallogr. Rep. 56 (2011) 1197.
[20] S.S. Arzumanov, et al., At. Energy 113 (2013) 351.
[21] S. Arzumanov, et al., in: ISINN-9, Dubna, 2001, p. 397.
[22] V.V. Nesvizhevsky, et al., Crystallogr. Rep. 58 (2013) 743.
[23] V.I. Morozov, Preprint IAE-6227/2, Moscow, 2001.